Journal of Power Sources 183 (2008) 26–33

Contents lists available at ScienceDirect

Journal of Power Sources

journal homepage: www.elsevier.com/locate/jpowsour

Synergistic effects of $Ni_{1-x}Co_x$-YSZ and $Ni_{1-x}Cu_x$-YSZ alloyed cermet SOFC anodes for oxidation of hydrogen and methane fuels containing H_2S

Catherine M. Grgicak[1], Malgosia M. Pakulska, Julie S. O'Brien, Javier B. Giorgi*

Centre for Catalysis Research and Innovation, Department of Chemistry, University of Ottawa, Ottawa, Ontario, Canada K1N 6N5

ARTICLE INFO

Article history:
Received 10 March 2008
Received in revised form 30 April 2008
Accepted 1 May 2008
Available online 7 May 2008

Keywords:
Solid oxide fuel cell
Anodes
Nickel-cobalt sulfide
Nickel-copper sulfide
Sulfur tolerance
Methane oxidation

ABSTRACT

Preparation and performance of bimetallic $Ni_{(1-x)}Co_x$-YSZ and $Ni_{(1-x)}Cu_x$-YSZ anodes were tested to overcome common deficiencies of carbon and sulfur poisoning in SOFCs. $Ni_{1-x}Co_xO$-YSZ and $Ni_{(1-x)}Cu_xO$-YSZ precursors were synthesized via co-precipitation of their respective chlorides. Single cell solid oxide fuel cells of these bimetallic anodes were tested in H_2, CH_4, and H_2S/CH_4 fuel mixtures. Addition of Cu^{2+} into the NiO lattice resulted in large metal particle sizes and decreased SOFC performance. Addition of Co^{2+} into the NiO lattice to form $Ni_{0.92}Co_{0.08}O$-YSZ anode precursor produced a cermet with a large BET surface area and active metal surface area, thus increasing the rate of hydrogen oxidation for this sample. The performance of both bimetallics was found to quickly degrade in dry CH_4 due to carbon deposition and lifting of the anode from the electrolyte. However, $Ni_{0.69}Co_{0.31}$-YSZ showed superior activity in a 10% (v/v) H_2S/CH_4 fuel mixture, surpassing performance with H_2 fuel, thereby demonstrating the exciting prospect of using sulfidated $Ni_{(1-x)}Co_x$-YSZ as SOFC anodes in sulfur containing methane streams. The active anode becomes a sulfidated alloy (Ni-Co-S) under operating conditions. This anode showed enhanced performance, which surpassed those of sulfidated Ni and Co anodes, thereby suggesting a synergistic behaviour in the Ni-Co-S anode.

1. Introduction

Nickel-yttria stabilized zirconia (Ni-YSZ) cermet is the most commonly used material for solid oxide fuel cell (SOFC) anodes because it satisfies the basic requirements of an anode material. Namely, metallic nickel serves as an excellent catalyst for the oxidation of hydrogen and provides electronic conductivity for the anode, while the thermal expansion coefficient of the nickel-based anode is managed by mixing it with YSZ [1–3].

Recent efforts towards improving SOFC performance and versatility have focused on finding novel anode materials to overcome the limitations of Ni-YSZ, the most important of which is its low tolerance for carbon and sulfur poisoning. Numerous efforts to sustain direct utilization of dry hydrocarbons in SOFCs have shown that conventional Ni-YSZ anodes are prone to uncontrolled carbon deposition during operation with these fuels since catalytic dissociative adsorption of CH_4 on the anode surface (Eq. (1)) competes with the desired electrochemical reaction (Eq. (2)).

$$CH_4 \rightarrow C_{(gr)} + 2H_2 \quad (1)$$

$$CH_4 + 4O^{2-} \rightarrow CO_2 + 2H_2O + 8e^- \quad (2)$$

Recent studies have attempted to circumvent carbon deposition by using alternative operating conditions, where steam is added to the fuel stream [4,5]. The anode provides catalytic sites for reforming CH_4 to H_2 and CO. However, internal steam reforming of methane is endothermic and can cause a significant cooling effect with the development of large temperature gradients, while the high H_2O/CH_4 ratio required to avoid coke formation results in a severe decrease of fuel cell open-circuit potential (OCV), thereby reducing its efficiency. An additional modification to the operating conditions has focused on introducing oxygen through the electrolyte by increasing the electrochemical load [6].

Other work has focused on preparing alternative anode materials which may be used directly in a dry hydrocarbon environment without changing the operating conditions. Alternative materials, which are easy to maintain as well as process and exhibit similar catalytic properties to those of Ni without suffering similar carbon formation, are currently being sought to replace Ni-based anodes. Emphasis has been placed on Cu-based anode materials since they are inexpensive and have been shown to be relatively inert to the formation of C—C bonds. However, the low melting temperature of

* Corresponding author. Tel.: +1 613 562 5800x6037; fax: +1 613 562 5170.
E-mail address: jgiorgi@uottawa.ca (J.B. Giorgi).
[1] Present address: Biomedical Forensic Sciences, Boston University School of Medicine, United States.

0378-7753/$ – see front matter © 2008 Elsevier B.V. All rights reserved.
doi:10.1016/j.jpowsour.2008.05.002

copper requires that the anodes be produced by pre-sintering the electrolytic component with pore formers prior to Cu impregnation [7]. Additives such as Mo, Pd, Co, Sm_2O_3 and CeO_2 to Ni- and Cu-based anodes have also been examined and show positive results as they inhibit the formation of adsorbed graphitic layers [8–11]. However, problems associated with cell processing/assembly and carbon formation are yet to be resolved.

An additional point to consider is the existence of fuel impurities in most hydrocarbon feed stocks (i.e. sulfur compounds), which cause degradation of the anodes, affecting the overall performance of the fuel cell. Therefore, it has been of interest to examine the sulfur tolerance of SOFC anodes by understanding the sulfur poisoning mechanism and to develop sulfur tolerant anodes for SOFC systems. Ni-YSZ-based systems have shown little tolerance to fuels containing low (ppm) H_2S concentrations, where sulfur tolerance decreases as a function of lower operating temperatures and higher H_2S concentrations [12,13]. However, up to 90% recovery of these systems was observed when H_2S was removed from the fuel, signifying that poisoning is caused by blocking of the active Ni-YSZ sites by either adsorbed sulfur or H_2S. The small irreversible component was suggested to be the result of Ni—S bond formation [13,14]. Further studies of nickel-sulfide interactions by Raman spectroscopy at high temperatures suggest that Ni-S is the prevalent species under these SOFC operating conditions [15].

Due to the incompatibility of Ni-YSZ-based systems with sulfur, recent emphasis has been placed on improving the tolerance of SOFC anodes by changing their composition. Ni-based anodes, where the electrolyte component was changed from yttria-stabilized zirconia (YSZ) to scandia-stabilized zirconia (SSZ) showed increased tolerance at a concentration of 100 ppm H_2S at 800 °C [12]. Cu-ceria anodes exhibited high sulfur tolerance and were able to operate at levels up to 450 ppm H_2S at 800 °C without any appreciable loss of performance [16]. An alternative approach was to utilize a perovskite structure, which can support oxide-ion vacancies to give good oxide-ion conduction and have a mixed-valent cation from the 4d or 5d block that provides good electronic conduction, while exhibiting high sulfur tolerance. The double perovskites $Sr_2Mg_{1-x}Mn_xMoO_{6-\delta}$ show long term stability in 50 ppm H_2S/H_2 at 800 °C, without the formation of sulfur species [17]. Other perovskites also show potential by exhibiting sulfur tolerance at 1000 °C for up to 8 h in a 1% H_2S/H_2 mixture [18]. Although these anode materials show promise in H_2S/H_2 fuel mixtures at low concentrations, little evidence for their long term performance at high sulfur concentrations is available.

The ability of an anode material to electrochemically oxidize H_2S in a fuel cell has also been established. This was first demonstrated by Pujare et al. by utilizing thiospinel $CuFe_2S_4$ as the anode's electrocatalytic site with pure H_2S as the fuel [19]. Additionally, anode catalysts comprising composite metal-sulfides derived from a mixture of Mo and other transition metal-sulfides (Fe, Co, Ni) were stable and effective electrocatalysts for the conversion of H_2S in SOFCs, where Co-Mo-S exhibited superior activity and longevity among those developed [20,21]. Although these results suggested that metal-sulfides are viable SOFC anodes for H_2S containing fuels, very little is understood regarding the H_2S oxidation reaction, which can proceed by multiple pathways giving rise to different OCV values.

By studying the product distribution of the H_2S, $Pt|((Ce_2)_{0.8})(SmO_{1.5})|Pt$, air system, Peterson and Winnick suggested that the complete oxidation of hydrogen sulfide to sulfur dioxide was the preferred product [22]. However, it was impossible to determine whether complete oxidation of hydrogen sulfide occurred directly or via the thermal decomposition of H_2S, producing H_2 and S_2 intermediates (Eqs. (3) and (4)). Experimental OCV values (~1 eV) suggested that H_2 is the active fuel for the fuel cell reaction [23,24].

$$H_2S \rightarrow H_2 + \tfrac{1}{2}S_2 \quad (3)$$

$$\tfrac{1}{2}S_2 + 2O^{2-} \rightarrow SO_2 + 4e^- \quad (4)$$

Recently, Ni-YSZ and Co-YSZ were shown to be effective in fuel streams of hydrogen and methane containing 1–10% (v/v) H_2S [23,24]. The formation of a bulk sulfide species due to the sulfur content in the fuel stream seemed to prevent degradation due to carbon and sulfur poisoning. Furthermore, performance of the sulfidated anodes in an atmosphere containing H_2S showed an enhancement of performance (higher current densities) over the traditional cermet operating with H_2 fuel.

The work presented here involves alternative preparations of SOFC anodes which overcome the deficiencies of anode poisoning by the alloying of an alternative component in the metal phase of the cermet taking advantage of the synergistic properties different metal solutions. The alloyed anode, $Ni_{(1-x)}M_x$-YSZ, may improve the anodes' performance by improving its mechanical, thermal, or chemical properties. The desired properties are defined by high surface area (small particle size), high thermal stability (resistance to sintering), resistance to oxidation, resistance to carbon and sulfur poisoning, and enhanced fuel-oxidation performance.

Previous studies of bimetallic anodes suggest that improved hydrogen oxidation rates and carbon deposition resistance are possible. Small additions of Fe (10%, w/w) had a significant positive influence on power generation of an SOFC in humidified H_2 at 800 °C, whereas Mn and Ag additions greatly decreased power densities due to enlarged iR losses on the anode side [25]. However, iron is easily oxidized at high overpotentials or high oxygen partial pressures and may, therefore, exhibit undesirable corrosive properties under these conditions.

In general the thermal stability and sinteractivities of cermets are expected to increase with melting temperature of the metal phase. Nickel and copper have melting points of 1728 and 1356 K, respectively. Consequently, addition of significant amounts of copper to Ni-YSZ cermets shows a decrease in surface area [26,27]. However, introducing a small amount of copper into the nickel cermet may result in anodes which exhibit resistance to carbon poisoning.

Alternatively, cobalt exhibits a melting point of 1768 K. Alloys of Ni-Co are expected to display high electrochemical activities and thermal stabilities, and would not require any unusual processing conditions. Additionally, cobalt possesses a higher oxidation resistance than nickel and is not likely to exhibit corrosive properties at high overpotentials or high oxygen partial pressures [28]. It was recently shown that the addition of a small amount of cobalt to nickel cermets resulted in an increased electrochemical activation energy and pre-exponential factor, suggesting a larger metal dispersion [25]. This work was corroborated by Ringuede et al., where the surface area of these samples increased from 26 to 33 $m^2\,g^{-1}$ when moderate amounts of cobalt were added to Ni-YSZ cermet synthesis [26]. Increased capacitance during H_2 oxidation was also observed with moderate cobalt fractions in Ni-YSZ, suggesting microstructural changes such as extension of the triple phase boundary (TPB) [28].

This study is concerned with the stability and structural properties of NiCu- and NiCo-YSZ anodes in H_2, CH_4 and 10% (v/v) H_2S/CH_4. Prepared bimetallic cermets and post-run anode materials were characterized with surface area, X-ray diffraction (XRD) and X-ray fluorescence (XRF). Emphasis was placed on electrochemical performance of each anode in H_2 and stability in CH_4 and H_2S/CH_4 over time, in particular, their resistance to poisoning factors.

2. Experimental

2.1. Sample preparation

YSZ supported metal oxide anode precursor materials (nominally 70%, w/w MO-YSZ) were prepared by dissolving appropriate amounts of $ZrCl_4$, Y_2O_3 (dissolved in 10 ml of 37%, w/w HCl) and $NiCl_2{\cdot}6H_2O$, $CuCl_2{\cdot}2H_2O$ or $CoCl_2{\cdot}6H_2O$ (Aldrich) in 165 ml of distilled water. In order to ensure YSZ phase purity and stability, the cermet materials were synthesized with 21 mol% YSZ [27]. The precipitation was achieved through the introduction of sodium hydroxide (Aldrich) until a pH of 13 was reached. Following precipitation, the product was filtered, washed three times with 500 ml of distilled water, and dried at 120 °C for 18 h. A portion of the dried product was then calcined at 750 °C for 2 h. The molar composition of the resulting material was determined experimentally using X-ray fluorescence to account for the partial solubility of the substituting metal. The synthesized material had the general formula $Ni_{(1-x)}M_xO$-YSZ (M = Cu or Co) in the oxidized form and becomes $Ni_{(1-x)}M_x$-YSZ upon reduction.

2.2. Characterization

Quantification of the bulk atomic composition of each material was obtained using a Philips PW2400/00 X-ray fluorescence (XRF) instrument that was calibrated with a concentration gradient of NiO, CuO, or Co_3O_4 in a mixture of ZrO_2 and Y_2O_3. Powder composition and crystallite sizes were determined by X-ray diffraction (XRD) (Phillips PW1830) using Cu Kα radiation with a wavelength of 1.54 Å. The scan range was measured from $2\Theta = 20°$ to 90° at a rate of $0.02° \, s^{-1}$. Crystalline phases were assigned using the Powder Diffraction File (PDF) database (ICCD, 2001, Dataset 1-51). Lattice parameters were measured after theta calibration with LaB_6 as an internal standard (NIST) and peak refinement was performed using Jade 6.1 software.

The BET surface area and average particle size of the calcined powders were determined after reduction in flowing H_2 (99.9%, Praxair) at 600 °C for 2 h using a Quantachrome Autosorb 1-C instrument. The average metal particle size was measured by obtaining the active metal surface area via chemisorption experiments with H_2 as the vector gas.

Sintering experiments were performed by uniaxially pelleting 500 mg of the calcined oxide powders with a pressure of 37 MPa to form 13 mm disks. The green densities of each powder were determined by dividing the cylindrical volume of the pellet by the mass. All of the disks were sintered in air up to a temperature of 1500 °C at intervals of 100 or 50 °C. At each interval, the change in length of the diameter of the pellet was recorded with digital callipers at four points on the pellet, approximately every 30°. The following Arrhenius type equation was used to determine the activation energy of densification:

$$\ln\left(\frac{dL/L_o}{T}\right) = A - \frac{n \cdot E_a}{RT} \quad (5)$$

where E_a is the activation energy of densification and n is a constant which encompasses all values that describe the sintering behaviour of solids. The constant n includes information on surface energy, atomic volume, grain boundary thickness, grain size, and diffusion coefficients for grain boundary and volume diffusion. Traditionally, the value of n has been estimated to be 0.5 for volume diffusion and 0.33 for grain-boundary diffusion [29,30].

2.3. Electrochemical testing of synthesized anodes

Fuel cell construction and validation of the electrochemical setup has previously been described in detail [23,24]. The following is a brief description of the salient points. The fuel cell was prepared by mixing Triton X-100 (Research Chemical Ltd.)/distilled water and 1 g of anode powder. The slurry (0.15 g) was coated onto an YSZ green-disk (Tosoh) and sintered to 1400 °C for 4 h in air. A 70% (w/w) LSM/30% (w/w) YSZ mixture (LSM, Nextech Materials; YSZ, Tosoh) was used as the cathode and reference electrode material. The cathode was prepared by coating 0.15 g of the LSM/YSZ slurry symmetrically opposing the sintered anode, while the reference electrode was approximately 4 mm to the side of the cathode [31]. Upon sintering, the YSZ electrolyte was 0.5 mm thick with electrode areas of 0.4 cm^2 for the anode and cathode and 0.2 cm^2 for the reference electrode. Both numerical and experimental findings suggest that the ideal three-electrode geometry for an SOFC would include a symmetric cell where the counter and working electrodes are symmetrically opposed to one another with the reference electrode as far away from them as possible [32,33]. Also, by increasing the electrolyte thickness, errors associated with electrode misalignment would be minimized. However, a compromise regarding electrolyte thickness is needed given that it must be thin enough to allow reasonable current densities, but thick enough to keep electrode alignment errors minimal [31]. A full depiction of the cell setup has previously been described [23].

The current collector was a Pt-10%Rh mesh with a 0.003 in. wire diameter (Unique Wire Weaving Co.) embedded into the electrodes. The current collector was embedded by adding an additional coat of anode slurry and sintering to 1400 °C. This process was used to minimize any losses due to contact resistance [34]. Although the active thickness of fine Ni-YSZ cermet anodes has been demonstrated to be in the range of 10 μm [35] while the rest of the anode acts as a current carrier, issues related to enhanced activity due to the mesh were nevertheless tested and found to have an insignificant impact on its performance [24]. Although Pt or Rh were not observed by EDS mapping in the active region, migration of these atoms cannot be fully ruled out. However, since the fabrication procedure was identical for all fuel cells, minor enhancements in activity should be comparable and the observed differences in fuel cell behaviour are attributed to differences in anode material properties.

All electrochemical measurements were performed in pure H_2, CH_4, or a 10% (v/v) H_2S/CH_4 mixture at 850 °C. All fuel flows were regulated by mass flow controllers (MKS) to a total, constant flow of 50 sccm. After initial preparation, mounting, and reduction of the single cell, a minimum OCV of 1.0 V was required to continue electrochemical measurements. All electrochemical measurements were obtained using a VoltaLab 40 (Radiometer Analytical). Impedance measurements were taken over a frequency range of 100 kHz to 250 mHz at OCV. Equivalent circuit modeling of the impedance data was performed with Zview software. DC current–voltage measurements were conducted using a potential scan rate of $2 \, mV \, s^{-1}$. Post-run analysis of the fuel cell anodes was accomplished by X-ray diffraction (XRD) using the same instrument, experimental parameters, and assignment database as outlined above. A NanoLab7 SEM with Kevex EDS was used for imaging and elemental analysis.

3. Results and discussion

3.1. Characterization of bimetallic SOFC anodes

Co-precipitation of $NiCl_2{\cdot}6H_2O$, Y_2O_3 and $ZrCl_2$ resulted in a two-phase mixture of cubic NiO and YSZ, with lattice parameters

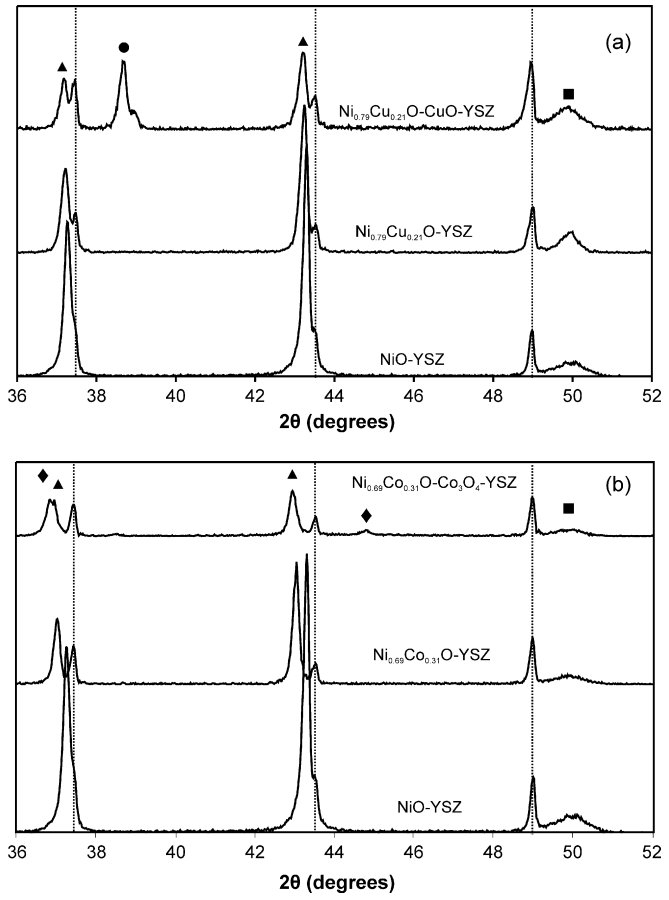

Fig. 1. XRD patterns of NiO-YSZ SOFC anode precursors synthesized with varying amounts of (a) Cu^{2+}: $Ni_{1-x}Cu_xO$-YSZ, $x = 0$, 0.21, 0.67; and (b) Co^{2+}: $Ni_{1-x}Co_xO$-YSZ, $x = 0$, 0.31, 0.60. Phases are indicated by: (▲) NiO (■) YSZ (●) CuO and (♦) Co_3O_4. Vertical lines indicate the LaB_6 internal standard peaks.

of 4.1761(0.0003) and 5.157(0.001) Å respectively as measured by XRD. Addition of small amounts of $CuCl_2{\cdot}2H_2O$ or $CoCl_2{\cdot}6H_2O$ as an additional reagent prior to precipitation did not introduce a third phase to the mixture. Although the two major phases remained NiO and YSZ a downward shift in the 2Θ position of the NiO peaks was observed, suggesting a solid solution between the NiO and the additive metal. Significant additions of $CuCl_2{\cdot}2H_2O$ or $CoCl_2{\cdot}6H_2O$ were required before segregate phases of CuO or Co_3O_4 were observed. Fig. 1 shows a portion of the diffractograms ($2\Theta = 36$–52°) for $Ni_{(1-x)}Cu_xO$-YSZ and $Ni_{(1-x)}Co_xO$-YSZ samples respectively; it illustrates 3 distinct points in the synthesis of powders with increasing Cu or Co additive concentration. Fig. 1a shows the NiO-YSZ spectra, a copper concentration near saturation ($Ni_{(1-x)}Cu_xO$-YSZ, $x = 0.21$) where the NiO peak is shifted, and a high concentration of additive metal (nominally $x = 0.68$) where a phase segregation is observed ($Ni_{(1-0.21)}Cu_{0.21}O$-CuO-YSZ). Similarly, Fig. 1b shows the NiO-YSZ spectra, a cobalt concentration near saturation ($Ni_{(1-x)}Co_xO$-YSZ, $x = 0.31$) where the NiO peak is shifted, and a high concentration of additive metal (nominally $x = 0.60$) where a phase segregation is observed ($Ni_{(1-0.31)}Co_{0.31}O$-Co_3O_4-YSZ). Separation of a cobalt oxide phase causes a change in the cobalt-oxygen stoichiometry, since the stable species observed is Co_3O_4 instead of CoO. Vertical lines in both panels indicate the positions of the LaB_6 internal standard peaks.

The variation of the cubic lattice parameters for all NiO samples with respect to copper and cobalt concentration as obtained from the XRD spectra is shown in Fig. 2. Variation of the NiO

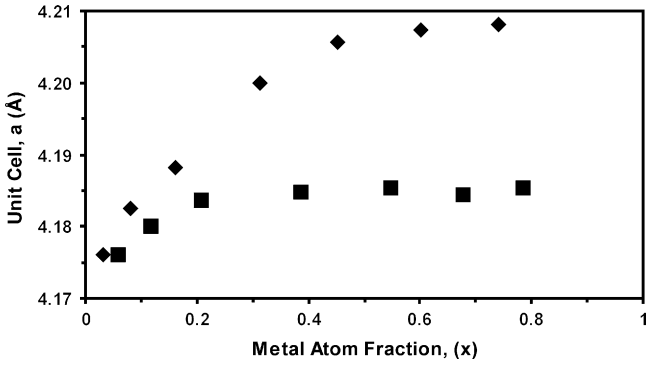

Fig. 2. Variation in cubic unit cell parameters of NiO in $Ni_{(1-x)}M_xO$-YSZ samples with increase in (■) Cu and (♦) Co content.

lattice parameter in the calcined sample was linear with copper content up to 8% (w/w) ($Ni_{(1-x)}Cu_xO$, $x = 0.21$). Once a higher amount of copper was added, the increase in lattice parameters of NiO reached a plateau and a separate monoclinic CuO phase was observed. This type of cell-parameter variation is typical of systems in which lattice substitution occurs. The observed variations of the lattice parameters at low copper concentrations were mainly due to the difference of ionic radii between the original and substituent metals, $R_{Ni^{2+}} = 0.69$ Å and $R_{Cu^{2+}} = 0.72$ Å [36]. The same trend is observed for nickel/cobalt samples; however, increases in NiO lattices were significantly larger for Co^{2+} than for Cu^{2+}, which were attributed to the larger ionic radius of Co^{2+} ($R_{Co^{2+}} = 0.74$ Å) [36]. Variation of the NiO lattice parameter was linear with Co content up to 24% (w/w) ($Ni_{(1-x)}Co_xO$, $x = 0.45$), suggesting that the solubility of Co^{2+} in the NiO lattice is greater than that of Cu^{2+}. Beyond this point, the lattice parameter did not change and a separate Co_3O_4 phase was observed in the diffractogram. The YSZ lattice parameters remained constant (5.162(0.003) Å) for every cermet system despite changes in the overall Cu^{2+} or Co^{2+} concentrations.

Table 1 shows the relative molar concentrations of metals in the two-phase mixtures determined by XRF, assuming full isomorphic substitution of Cu^{2+} or Co^{2+} in NiO. Mixtures with the presence of a third phase (CuO or Co_3O_4) are not included. The BET surface area of NiO-YSZ was 31 $m^2\,g^{-1}$ with an average Ni particle size of 253 nm. Substitution of Cu^{2+} within the oxide significantly reduced the surface area and increased the particle size of the alloy. This is an undesired effect because it causes the active area for fuel oxidation to be reduced. The repercussions of this effect on anode performance will be discussed in the following sections. Substitution of Co^{2+} shows a similar behaviour, except for the smallest Co concentration $Ni_{0.92}Co_{0.08}O$-YSZ which shows a slight increase in surface area.

Table 1
Powder characteristics of single and alloyed metal SOFC anode precursors

Formula composition of metal oxide phase[a]	BET surface area of reduced powder ($m^2\,g^{-1}$)	d_{Metal} (nm)[b]	E_a (kJ mol^{-1})
NiO	31	253	870 ± 40
$Ni_{0.88}Cu_{0.12}O$	16	677	380 ± 20
$Ni_{0.79}Cu_{0.21}O$	12	3576	470 ± 50
CuO	12	1261	n/a
$Ni_{0.92}Co_{0.08}O$	44	118	360 ± 40
$Ni_{0.84}Co_{0.16}O$	22	770	420 ± 10
$Ni_{0.69}Co_{0.31}O$	19	2143	460 ± 20
Co_3O_4	18	240	600 ± 10

n/a: not applicable since CuO-YSZ melts at ~1100 °C.
[a] Formula compositions were determined by XRF.
[b] BET surface area and d_{Metal} were obtained on reduced precursor powders previously calcined to 750 °C.

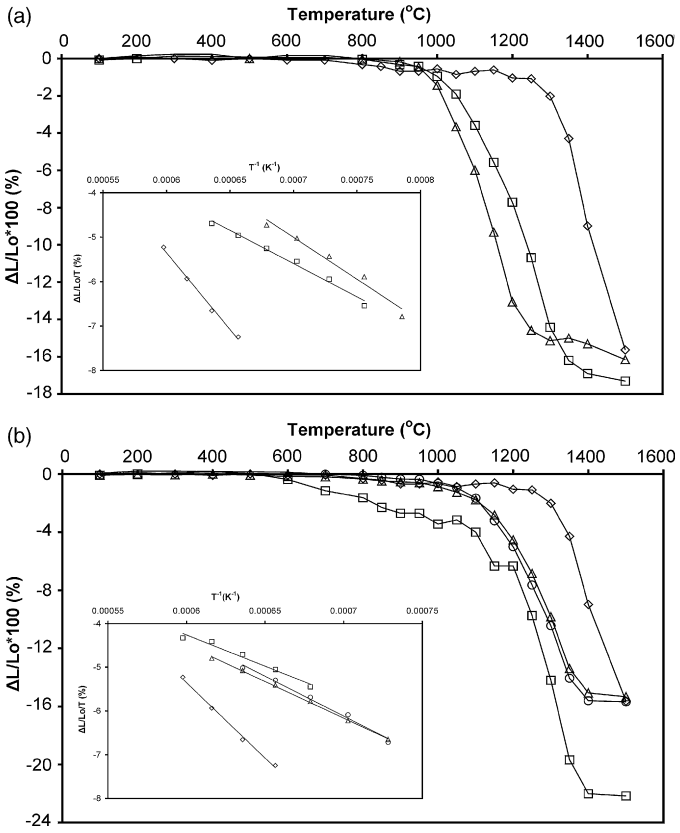

Fig. 3. Shrinkage characteristics of each sample as a function of temperature. (a) (◊) NiO-YSZ (□) $Ni_{0.88}Cu_{0.12}O$-YSZ, (△) $Ni_{0.79}Cu_{0.21}O$-YSZ. (b) (◊) NiO-YSZ, (□) $Ni_{0.92}Co_{0.08}O$-YSZ, (△) $Ni_{0.84}Co_{0.16}O$-YSZ, (○) $Ni_{0.69}Co_{0.31}O$-YSZ. Inset: Determination of the activation energy of sintering for each sample using the Arrhenius relationship.

Sintering activity was also affected by the addition of copper or cobalt. The sintering behaviour of these two types of powders was significantly different despite their identical green densities ($3.0 + 0.2\,g\,cm^{-3}$). Fig. 3 shows the observed shrinkage as a function of temperature for the two-phase samples. The temperature for maximum reduction in size shifts continuously towards lower temperature for the $Ni_{(1-x)}Cu_xO$-YSZ samples, while the $Ni_{(1-x)}Co_xO$-YSZ samples only show changes in slope.

These differences are related to the activation energy of shrinkage, which is derived from the combined-stage sintering model (Eq. (5)). The insets of Fig. 3 show the rate of shrinkage for each metal or alloy within the linear region. The predominant mechanism was assumed to be grain boundary diffusion ($n = 0.33$) based on the mechanism attributed to the sintering of 8% YSZ [37]. Initially, the sintering activation energy decreased from 870 + 40 to $380 + 20\,kJ\,mol^{-1}$ for NiO-YSZ and $Ni_{0.88}Cu_{0.12}O$-YSZ respectively despite the larger metal particle size associated with this sample and is a direct result of Cu^{2+} substitution within the NiO lattice (Fig. 3a). Increasing the copper concentration resulted in an increase of metal particle size and a decrease of sintering activity. The same trend was apparent for the $Ni_{(1-x)}Co_xO$-YSZ samples, showing smaller sintering activities than those of the single metal cermets (Fig. 3b). As the concentration of cobalt increased within the alloys, particle sizes increased while sintering activities decreased. The values for the activation energies of sintering are tabulated in Table 1. The decrease in sintering activation energies is an undesired effect of the alloy formation. Sintering activities play an important role in the optimization of the anodes' microstructure, which has repercussions toward the performance of the anode.

Overall, $Ni_{(1-x)}M_xO$-YSZ (M = Cu or Co) materials prepared by the precipitation technique show material properties which appear less desirable for their application as precursors for anodes in SOFC than those of NiO-YSZ. However, optimization of the preparation for microstructure has not been performed, and the reactivity of the alloys under operating conditions has the potential to offset the limitations in microstructure (*vide infra*).

3.2. Anode performance

3.2.1. Performance with H_2 and H_2S/H_2 fuels

Determination of the exchange current density for each anode was obtained by using the high field approximation of the generalized kinetic equation for electron transfer processes proposed by Erdey-Gruz and Volmer and Butler [38–41]. Corrections for iR_s were made by utilizing the high frequency intercept from impedance measurements at OCV. The exchange current densities were used to evaluate the performance differences of the various anode materials. Fig. 4 shows an example of iR_s corrected DC measurements for the $Ni_{0.92}Co_{0.08}$-YSZ (Fig. 4a) and $Ni_{0.69}Co_{0.31}$-YSZ (Fig. 4b) anodes in H_2 and 10% (v/v) H_2S/CH_4 ($t = 15$ h) as well as the Tafel fits for each. The ln(i) response is shown every 25 mV for clarity.

The overpotential range was not restricted since there was no indication of passivation. The Tafel region was calculated between 400–550 mV for samples run in H_2, but spanned a much larger overpotential region. The Tafel region for samples run in CH_4/H_2S also spanned 150 mV, but at higher overpotentials (i.e. −600 mV) since there is an anodic peak which disallows for linear extrapolation at smaller overpotentials. The exchange current density at OCV is obtained from the intercept of the Tafel fit. Since the Butler-Volmer equation assumes that the electrochemical activation is directly related to changes in the electrochemical free energy of the system, mass diffusion or adsorption effects were considered. Previous

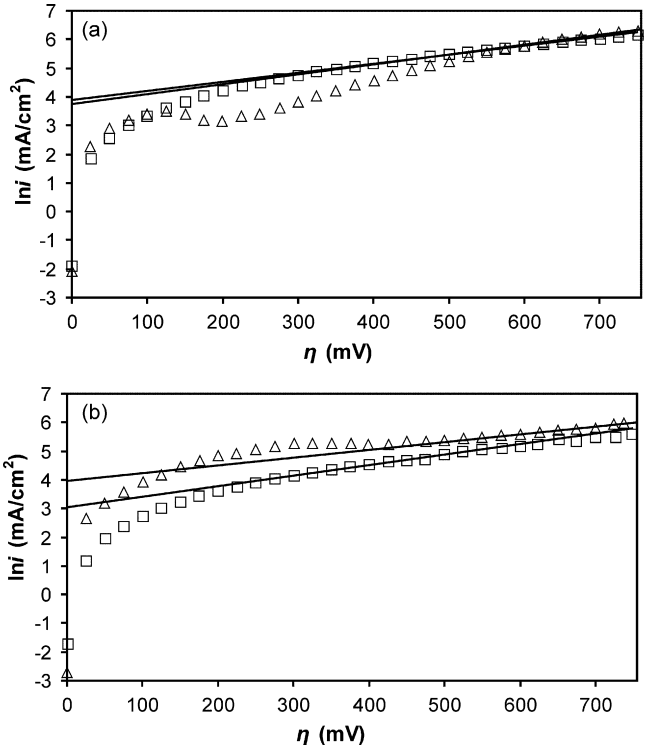

Fig. 4. Example ln(i)–potential relations on sample (a) $Ni_{0.92}Co_{0.08}$-YSZ and (b) $Ni_{0.69}Co_{0.31}$-YSZ used to determine exchange current densities for samples in (□) H_2 and (△)10% (v/v) H_2S/CH_4 atmospheres.

Table 2
Exchange current densities for $Ni_{(1-x)}Cu_x$- and $Ni_{(1-x)}Co_x$-YSZ anodes in hydrogen

Metal-YSZ anode	i_o (mA cm^{-2})	Standard deviation of i_o (mA cm^{-2})
Ni	14	6
$Ni_{0.88}Cu_{0.12}$	17	6
$Ni_{0.79}Cu_{0.21}$	2	n/a
Cu	0.16	0.04
$Ni_{0.92}Co_{0.08}$	48	13
$Ni_{0.84}Co_{0.16}$	15	3
$Ni_{0.69}Co_{0.31}$	28	4
Co	5	1

n/a: not applicable.

studies in this laboratory indicated the electrochemical responses were due to charge transfer reactions and not adsorption or diffusion processes. More specifically, impedance spectroscopy showed the third low frequency response, which is usually attributed to 'gas conversion', was not observed at $\eta > 200$ mV, suggesting simple gas diffusion limitations based on Fick's Law should not be used to describe this element. Furthermore, activation energies (90 ± 10 kJ mol^{-1} for Ni-YSZ and 130 ± 10 kJ mol^{-1} for Co-YSZ) calculated using this technique also suggested that the electrochemical responses were due to charge transfer reactions [23].

Exchange current density plots similar to Fig. 4 were obtained for all of the two-phase anode fuel cells ($Ni_{(1-x)}M_x$-YSZ) as well as for Ni-YSZ, Cu-YSZ, and Co-YSZ. The exchange current densities are summarized in Table 2 for the performance of each fuel cell. Addition of copper to the nickel cermet resulted in a marked decrease in performance, particularly for $Ni_{0.79}Cu_{0.21}$-YSZ. The decrease in performance is associated with the decreased TPB, which correlates with the large metal particles obtained in this sample [42]. In general, copper addition does not result in an improvement in performance due to its material properties and the stringent temperature requirements of the fuel cell preparation process.

In contrast, addition of cobalt shows improvement in fuel cell performance. In particular, $Ni_{0.92}Co_{0.08}$-YSZ showed significant improvement in anode performance when compared to Ni-YSZ and other $Ni_{(1-x)}Co_x$-YSZ samples. This was attributed to the larger surface area and smaller metal particle size obtained when moderate amounts of cobalt were introduced into the Ni lattice. This result is in agreement with Ringuede et al., who observed an increase in capacitance for moderate Co fractions, suggesting microstructural changes such as an extension of the metal/YSZ contact area [28].

The changes in performance upon addition of Cu or Co to Ni-YSZ anodes can also be discussed in terms of the catalytic activity of each metal. Recent modelling by Mukherjee and Linic suggests that the electrochemical oxidation of hydrogen at SOFC operating conditions would be more efficient on Co and Ni than on Cu anodes [43]. In fact, analysis of multiple metal catalysts shows a volcano-type plot with Co and Ni on either side of the maximum activity, suggesting a possible synergistic effect between these two metals.

3.2.2. Performance with CH_4 and H_2S/CH_4 fuels

Previous work using single metal M-YSZ anodes showed that upon operation with dry methane, the Ni-YSZ anode initially exhibited a slight increase in performance, but quickly degraded after 5 h of operation [24]. By the 15th hour, the anode had fully degraded and showed no activity. Post-run analysis showed that the anode had disintegrated and a black powder was observed at the bottom of the fuel cell. Co-YSZ exhibited an $i_oCH_4/i_oH_2 < 1$ at all times with no signs of decreasing performance during 15 h of testing. Post-run analysis of this anode showed it was separated from the electrolyte at the edges due to the onset of carbon poisoning and was expected to suffer full degradation with continued operation.

The $Ni_{(1-x)}Co_x$-YSZ samples in this work exhibited a similar trend for their carbon-poisoning behaviour as was found for the Ni- and Co-YSZ anodes. Carbon poisoning was prevalent for all $Ni_{(1-x)}Co_x$-YSZ anodes, with significant amounts of graphite found at the anode and at the bottom of the fuel cells, consistent with previous findings [11]. $Ni_{(1-x)}Cu_x$-YSZ anodes also showed significant carbon poisoning after 15 h. Although copper is relatively inert towards C—C bond formation, the presence of carbon degradation in these anodes suggested that the formation of a $Ni_{(1-x)}Cu_x$ alloy for $x < 0.21$ was insufficient to suppress carbon formation. That is, as found in the literature, a separate copper phase is needed to successfully oxidize dry methane at an appreciable rate, with little to no graphite formation [7,44].

When H_2S was added to the fuel mix, a marked change in performance behaviour was observed. With 10% (v/v) H_2S/CH_4 as a fuel, a decrease in performance was initially observed. However, the performance quickly increased and equalled or exceeded that observed with pure H_2 as the fuel. Table 3 shows the exchange current densities for fuel cells after 15 h of operation in H_2 and which were then exposed to H_2S/CH_4. $Ni_{0.92}Co_{0.08}$-YSZ and $Ni_{0.84}Co_{0.16}$-YSZ showed sufficient activities in H_2S/CH_4 fuel streams, resulting in exchange current densities which were approximately equivalent to those obtained when dry hydrogen was used, without any signs of degradation. Most impressively, $Ni_{0.69}Co_{0.31}$-YSZ exhibited a significant improvement in performance, where i_o increased from 24 mA cm^{-2} in H_2 to 94 mA cm^{-2} in H_2S/CH_4, representing a 4-fold improvement. Furthermore, $Ni_{0.69}Co_{0.31}$-YSZ showed superior performance in H_2S/CH_4, with an exchange current density surpassing all other anodes, even Ni-YSZ and Co-YSZ, suggesting that Ni and Co show a synergistic effect.

To analyse the origin of the improved behaviour of the alloy anodes, a qualitative analysis of the voltamograms is necessary. Near OCV, anodic peaks were observed in H_2S/CH_4 atmospheres, which were not present with H_2 as the fuel. This is particularly obvious for $Ni_{0.92}Co_{0.08}$-YSZ (representative of all samples, and shown in Fig. 4a). Previous cyclic voltammetry (CV) experiments performed in this laboratory on M-YSZ samples show that the process observed at $\eta = 200$–400 mV was irreversible in H_2S atmospheres [23]. CV studies at various operating conditions are required to fully determine the nature of these peaks; however, previous studies using Cu_2S anodes by Nava and Gonzalez suggest that they may be related to serial oxidation of the metal-sulfides through defective sulfides [45]. Bai and Conway showed that the shape of the observed feature depends on the complex kinetics of the system (compare Fig. 4a and b). The shape depends on the reactions (parallel vs. consecutive), their relative rates and equilibrium potentials of the individual steps [46]. A quantitative electrochemical analysis will be required to model the full shape of the voltamogram.

The stability of the alloy anode performance in H_2S/CH_4 fuel can be discussed in terms of the exchange current density. All anodes were run in sulfur containing fuel for 15 h. Similarly to the single metal-based anodes, M-YSZ [24], the value of i_o varied during the first 3–5 h likely due to the formation of the sulfidated species, and then became stable. $Ni_{0.69}Co_{0.31}$-YSZ reaches a maximum exchange current density of 216 mA cm^{-2} after 3 h and then stabilizes to $\sim$100 mA cm^{-2} after 5 h.

3.2.3. Run and post-run analyses

XRD analysis of post-run anodes indicated that the presence of high levels of H_2S in the fuel stream resulted in anodes consisting of metal-sulfide species. The process of forming a metal-sulfide species was deemed to be the cause of the initial decrease in performance. Once all of the metal was converted to metal-sulfide, a marked increase in performance was observed. This behaviour is similar to that previously observed for single metal, M-YSZ [23,24].

Table 3
Comparison of exchange current densities of individual fuel cells run in H_2 and then in H_2S/CH_4

Formula composition of metal oxide precursor phase	i_o (mA cm^{-2}) in dry H_2	i_o (mA cm^{-2}) in 10% (v/v) H_2S/CH_4	$\frac{i_o H_2S/CH_4}{i_o H_2}$
NiO	18	32	1.8
$Ni_{0.92}Co_{0.08}O$	51	44	0.9
$Ni_{0.84}Co_{0.16}O$	13	12	0.9
$Ni_{0.69}Co_{0.31}O$	24	94	3.9
Co_3O_4	4	25	6

Three phases were observed in the XRD of the post-run anodes. The phases were associated with Co-substituted Ni_3S_2 (PDF# 44-1418), Ni_7S_6 (PDF# 14-0364), and a minor unidentified phase. SEM/EDX spot analysis showed that all areas of the post-run anodes contained Ni, Co, and S species as well as YSZ particles. No single-metal-sulfide (NiS-, CoS-) areas were observed by EDX. Therefore, sulfidation of the $Ni_{1-x}Co_x$ alloy appears to promote alloy sulfide species and not single metal-sulfide phase separation, suggesting the active species during H_2S/CH_4 SOFC operation is a NiCoS species.

Observation of multiple phases in the post-run anodes is not unexpected. The phase diagram of Ni-S is complex and the species present after cooling a high temperature sulfide depend also on the rate of cooling [47,48]. Recent calculations have predicted that the stable phase under SOFC conditions is an "adsorbed-sulfur on nickel" species [49]. Such species, consisting of an intermediate between nickel metal and Ni_3S_2, explain the poisoning results observed at low H_2S concentrations, but cannot predict the enhanced performance observed in this work at higher H_2S concentrations. At this time, it was not possible to determine if the active phase during fuel cell operation is one of the observed phases (post mortem) or a distinct phase that exists only at high temperature. In situ experiments would be required to make this determination.

Analysis of exhaust gas by mass spectrometry indicated that there was not a significant amount of SO_2 produced, yet there was CS_2 production according to Eq. (6).

$$CH_4 + 2H_2S \rightarrow CS_2 + 4H_2 \quad (6)$$

Other possible products such as CH_3SH and C_2H_5SH were not observed in the mass spectrum [50]. Additionally a silvery foil-like substance was found near the anodes and along the edges of the alumina tube. Characterization of the foil showed it was amorphous with flat plate-like particles approximately 10 μm in diameter. XPS studies revealed the surface region was composed of carbon, oxygen, and sulfur [24].

OCV values obtained for all systems were 1.0 ± 0.1V, preventing the electrochemically active species from being distinguished between H_2, CH_4, or CS_2. However, increased activity of the systems run with sulfur-containing fuel with respect to H_2 demonstrated the exciting prospect of using bimetal-sulfides as anodes for oxidation of sulfur containing natural gas. This is particularly true for sulfidized $Ni_{0.69}Co_{0.31}$YSZ, which showed superior activity in 10% (v/v) H_2S/CH_4.

$Ni_{(1-x)}Cu_x$-YSZ samples were tested in H_2S/CH_4, but exhibited mechanical stress (i.e. electrolyte cracking) during the first few hours of operation, which suggests that the expansion mismatch between anode and electrolyte was too great during sulfidation of $Ni_{(1-x)}Cu_x$.

4. Conclusions

Co-precipitation of the appropriate metal chlorides with NaOH to pH 13 was used to prepare various bimetallic SOFC anode materials. The substitution of Cu^{2+} into the NiO lattice resulted in larger particle sizes, and smaller sinteractivities. Fuel cell performance was negatively affected by Cu^{2+} substitution into the NiO lattice. The resulting $Ni_{(1-x)}Cu_x$-YSZ anode showed decreased exchange current densities with increasing copper content due to changes in microstructure and activity. The addition of moderate amounts of copper did not inhibit graphite formation during dry methane oxidation.

The substitution of Co^{2+} into the NiO lattice resulted in powders with increased surface areas and decreased metal particle sizes, providing a significant, positive effect on the sinteractivities and performance of the resulting SOFCs. $Ni_{0.92}Co_{0.08}$-YSZ showed improved performance for H_2 oxidation. This increase was attributed to the extension of the TPB. $Ni_{0.69}Co_{0.31}$-YSZ showed superior performance in H_2S/CH_4 streams compared to pure H_2, suggesting sulfidated $Ni_{0.69}Co_{0.31}$-YSZ is a superior electrocatalyst for sulfur and carbon containing fuels. The synergy between nickel and cobalt in sulfidated nickel-cobalt anodes needs to be further explored.

Acknowledgements

The authors thank the Natural Sciences and Engineering Research Council of Canada (NSERC) and the Ontario Research Fund for financial support.

References

[1] N.Q. Mihn, J. Am. Ceram. Soc. 76 (1993) 563–588.
[2] W. Zhu, S. Deevi, Mater. Sci. Eng. A362 (2003) 228–239.
[3] Y.M. Park, G.M. Choi, Solid State Ionics 120 (1999) 265–274.
[4] J. Liu, S.A. Barnett, Solid State Ionics 158 (2003) 11–16.
[5] A. Weber, B. Sauer, A.C. Muller, D. Herbstritt, E. Ivers-Tiffee, Solid State Ionics 152–153 (2002) 543–550.
[6] J.-H. Koh, Y.-S. Yoo, J.-W. Park, H.C. Lim, Solid State Ionics 149 (2002) 157–166.
[7] R.J. Gorte, S. Park, J.M. Vohs, C. Wang, Adv. Mater. 12 (2000) 1465–1469.
[8] N.C. Triantafyllopoulos, S.G. Neophytides, J. Catal. 217 (2003) 324–333.
[9] Z. Zhan, Y. Lin, S. Barnett, in: S.C. Singhal, J. Mizusaki (Eds.), Proceedings of Electrochemical Society. SOFC IX, vol. 2, The Electrochemical Society, Inc., Quebec City, Quebec, 2005, pp. 1321–1329.
[10] Y. Nabae, I. Yamanaka, S. Takenaka, M. Hatano, K. Otsuka, in: S.C. Singhal, J. Mizusaki (Eds.), Proceedings of Electrochemical Society. SOFC IX, vol. I2, The Electrochemical Society, Inc., Quebec City, Quebec, 2005, pp. 1341–1351.
[11] K. Ahn, S. Lee, J. Vohs, R. Gorte, in: S.C. Singhal, J. Mizusaki (Eds.), Proceedings of Electrochemical Society. SOFC IX, vol. 2, The Electrochemical Society, Inc., Quebec City, Quebec, 2005, pp. 1360–1368.
[12] K. Sasaki, K. Susuki, A. Iyoshi, M. Uchimura, N. Imamura, H. Kusaba, Y. Teraoka, H. Fuchino, K. Tsujimoto, Y. Uchida, N. Jingo, in: S. Singhal, J. Mizusaki (Eds.), Proceedings of Electrochemical Society. SOFC IX, vol. 2, The Electrochemical Society, Inc., Quebec City, Quebec, 2005, pp. 1267–1274.
[13] Y. Matsuzaki, I. Yasuda, Solid State Ionics 132 (2000) 261–269.
[14] S. Xia, V. Birss, in: S.C. Singhal, J. Mizusaki (Eds.), Proceedings of Electrochemical Society. SOFC IX, vol. 2, The Electrochemical Society, Inc., Quebec City, Quebec, 2005, pp. 1275–1283.
[15] J. Dong, S. Zha, M. Liu, in: S.C. Singhal, J. Mizusaki (Eds.), Proceedings of Electrochemical Society. SOFC IX, vol. 2, The Electrochemical Society, Inc., Quebec City, Quebec, 2005, pp. 1284–1293.
[16] H. He, R.J. Gorte, J.M. Vohs, Electrochem, Solid State Lett. 8 (2005) A279–A280.
[17] Y.H. Huang, R.I. Dass, Z.-L. Xing, J.B. Goodenough, Science 312 (2006) 254–257.
[18] R. Mukundan, E.L. Brosha, R.H. Garzon, Electrochem. Solid State Lett. 7 (2004) A5–A7.
[19] N.U. Pujare, K.W. Semkow, A.F. Sammells, J. Electrochem. Soc. 134 (1987) 2639–2640.
[20] M. Liu, G. Wei, J. Luo, A.R. Sanger, K.T. Chuang, J. Electrochem. Soc. 150 (2003) A1025–A1029.

[21] G. Wei, J. Luo, A. Sanger, K. Chuang, J. New Mater. Electochem. Syst. 8 (2005) 59–64.
[22] D.R. Peterson, J. Winnick, J. Electrochem. Soc. 145 (1998) 1449–1454.
[23] C.M. Grgicak, J.B. Giorgi, J. Phys. Chem. C 111 (2007) 15446–15455.
[24] C.M. Grgicak, R.G. Green, J.B. Giorgi, J. Power Sources 179 (2008) 317–328.
[25] T. Ishihara, J. Yan, M. Shinagawa, H. Matsumoto, Electrochim. Acta 52 (2006) 1645–1650.
[26] A. Ringuede, J. Labrincha, J. Frade, Solid State Ionics 141–142 (2001) 549–557.
[27] C.M. Grgicak, J.B. Giorgi, in: S.C. Singhal, J. Mizusaki (Eds.), Proceedings of Electrochemical Society. SOFC IX, vol. 2, The Electrochemical Society, Inc., Quebec City, Quebec, 2005, pp. 1200–1209.
[28] A. Ringuede, D. Bronine, J. Frade, Electrochim. Acta 48 (2002) 437–442.
[29] F. Tietz, F.J. Dias, D. Simwonis, D. Stover, J. Eur. Ceram. Soc. 20 (2000) 1023–1034.
[30] H. Su, D.L. Johnson, J. Am. Ceram. Soc. 79 (1996) 3199–3210.
[31] V.V. Krishnan, S. McIntosh, R.J. Gorte, J.M. Vohs, Solid State Ionics 166 (2004) 191–197.
[32] J. Winkler, P. Hendriksen, N. Bonanos, M. Mogensen, J. Electrochem. Soc. 145 (1998) 1184–1192.
[33] S. Chan, X. Chen, K. Khor, J. Appl. Electrochem. 31 (2001) 1163–1170.
[34] S. Jiang, J. Love, L. Apateanu, Solid State Ionics 160 (2003) 15–26.
[35] M. Brown, S. Primdahl, M. Mogensen, J. Electrochem. Soc. 2 (2000) 475–484.
[36] R. Shannon, Acta Crystallogr. (1976) 751–767.
[37] I. Gibson, G. Dransfield, J. Irvine, J. Mater. Sci. 33 (1998) 4297–4305.
[38] J. Butler, Trans. Faraday Soc. 19 (1923) 729–733.
[39] J. Butler, Trans. Faraday Soc. 28 (1932) 379–382.
[40] T. Erdey-Gruz, M. Volmer, Z. Phys. Chem. A 150 (1930) 203–213.
[41] T. Erdey-Gruz, H. Wick, Z. Phys. Chem. A 162 (1932) 53–62.
[42] C.M. Grgicak, R.G. Green, J.B. Giorgi, J. Mater. Chem. 16 (2006) 885–897.
[43] J. Mukherjee, S. Linic, J. Electrochem. Soc. 154 (2007) B919–B924.
[44] Z. Lu, L. Pei, T.-m. He, X.-q. Huang, Z.-g. Liu, Y. Ji, X.-h. Zhao, W.-h. Su, J. Alloys Compd. 334 (2002) 299–303.
[45] D. Nava, I. Gonzalez, Electrochim. Acta 51 (2006) 5295–5303.
[46] L. Bai, B.E. Conway, J. Electrochem. Soc. 137 (1990) 3737–3747.
[47] T. Rosenqvist, J. Iron Steel Inst. (1954) 37–57.
[48] Z. Cheng, M. Liu, Solid State Ionics 178 (2007) 925–935.
[49] J.-H. Wang, M. Liu, Electrochem. Commun. 9 (2007) 2212–2217.
[50] F. Raulin, G. Toupance, Origins Life 6 (1975) 91–97.